Monthly Notices
of the
ROYAL ASTRONOMICAL SOCIETY

MNRAS **479,** 4271–4277 (2018)
Advance Access publication 2018 July 4

doi:10.1093/mnras/sty1766

The two ultraluminous X-ray sources in the galaxy NGC 925

F. Pintore,[1]★ L. Zampieri,[2] S. Mereghetti,[1] A. Wolter,[3] G. Rodríguez,[4] G. L. Israel,[4] P. Esposito,[5] S. Paiano,[2] G. Trinchieri[3] and P. Ochner[2]

[1]*INAF – IASF Milano, Via E. Bassini 15, I-20133 Milano, Italy*
[2]*INAF – Osservatorio Astronomico di Padova, Vicolo dell'Osservatorio 5, I-35122 Padova, Italy*
[3]*INAF – Osservatorio Astronomico di Brera, Via Brera 28, I-20121 Milano, Italy*
[4]*INAF – Osservatorio Astronomico di Roma, Via Frascati 44, I-00040 Monteporzio Catone, Italy*
[5]*Anton Pannekoek Institute for Astronomy, University of Amsterdam, Science Park 904, NL-1098 XH Amsterdam, the Netherlands*

Accepted 2018 June 30. Received 2018 June 30; in original form 2018 May 4

ABSTRACT

NGC 925 ULX-1 and ULX-2 are two ultraluminous X-ray sources (ULXs) in the galaxy NGC 925, at a distance of 8.5 Mpc. For the first time, we analysed high quality, simultaneous *XMM–Newton* and *NuSTAR* data of both sources. Although at a first glance ULX-1 resembles an intermediate mass black hole candidate (IMBH) because of its high X-ray luminosity [$(2–4) \times 10^{40}$ erg s^{-1}] and its spectral/temporal features, a closer inspection shows that its properties are more similar to those of a typical super-Eddington accreting stellar black hole and we classify it as a 'broadened disc' ULX. Based on the physical interpretation of this spectral state, we suggest that ULX-1 is seen at small inclination angles, possibly through the evacuated cone of a powerful wind originating in the accretion disc. The spectral classification of ULX-2 is less certain, but we disfavour an IMBH accreting at sub-Eddington rates as none of its spectral/temporal properties can be associated with either the soft or the hard state of Galactic accreting black hole binaries.

Key words: accretion, accretion discs – stars: neutron – galaxies: individuals: NGC 925 – X-rays: binaries – X-rays: individual: NGC 925 ULX-1, NGC 925 ULX-2.

1 INTRODUCTION

Ultraluminous X-ray sources (ULXs) are extragalactic, point-like objects characterized by very high X-ray luminosities in the range 10^{39}–10^{42} erg s^{-1} (e.g. Fabbiano 1989; Feng & Soria 2011; Kaaret, Feng & Roberts 2017). Observational pieces of evidence suggest that ULXs are accreting X-ray binaries (XRBs) with massive donors (e.g. Liu et al. 2013; Motch et al. 2014). The ULX luminosities can be produced from super-Eddington accretion on stellar-origin black holes (BHs) that could be similar to the Galactic ones (e.g. Gladstone, Roberts & Done 2009; Sutton, Roberts & Middleton 2013b; Middleton et al. 2015) or moderately more massive (e.g. Zampieri & Roberts 2009). Alternatively, a possibility can be sub-Eddington accretion on to intermediate mass BHs (IMBHs; e.g. Colbert & Mushotzky 1999; Madau & Rees 2001; Miller & Hamilton 2002; Portegies Zwart et al. 2004), or super-Eddington accretion on to neutron stars (NSs; e.g. Bachetti et al. 2013; Israel et al. 2017a). The combination of spectral and temporal properties of ULXs should in principle allow the distinction between the nature and mass of the different accretors. In fact, IMBHs accreting sub-Eddington should present the hallmarks of the accreting states of Galactic BH binary systems (i.e. *hard* and *soft* states; McClintock & Remillard 2006), while super-Eddington accreting stellar BHs and NSs would more likely show the features of the *ultraluminous state* (see e.g. Roberts 2007; Gladstone et al. 2009). The latter is characterized spectrally by a curvature at energies of 2–5 keV, often associated with a thermal soft excess below ∼0.5 keV (e.g. Gladstone et al. 2009; Bachetti et al. 2013; Caballero-Garcia, Belloni & Wolter 2013; Walton et al. 2013a, 2014; Rana et al. 2015), and temporally by random short-term variability (e.g. Heil, Vaughan & Roberts 2009; Sutton et al. 2013b; Pintore et al. 2014). The high energy curvature may arise either from a cold, optically thick corona lying above an accretion disc (e.g. Poutanen et al. 2007; Gladstone et al. 2009; Pintore & Zampieri 2012), or (i) from the innermost region of an advection-dominated accretion disc (e.g. Mizuno et al. 2007), (ii) from the reprocessing of hard photons by an optically thick outflow, (iii) from a combination of these effects. The soft component may instead originate from the photosphere of a radiatively driven and clumpy wind ejected from the accretion disc (e.g. Pinto, Middleton & Fabian 2016) when the local luminosity at the surface overcomes the Eddington limit, as expected for super-Eddington accretion rates (e.g. Poutanen et al. 2007; Ohsuga et al. 2009; Takeuchi, Ohsuga & Mineshige 2013). These powerful outflows may also be responsible

★ E-mail: fabio.pintore@inaf.it

for the unpredictable ULX short-term variability (e.g. Middleton et al. 2015).

The discovery of four pulsating ULXs (PULXs) in M82 ULX-2, NGC 5907 X-1, NGC 7793 P13, and NGC 300 ULX-1 (Bachetti et al. 2014; Fürst et al. 2016, 2017; Israel et al. 2017a,b; Carpano et al. 2018) demonstrated that ULXs can contain NSs, indicating clearly that the ULX population does not host only BHs. Furthermore, the PULXs enlarged our view of the accretion physics in ULXs and, in general, of the extreme mechanisms that can power accreting NSs. The four PULXs currently represent the most super-Eddington accreting sources. Their spectral and temporal properties are similar to other well-studied ULXs, although they may have a harder emission (e.g. Pintore et al. 2017; Walton et al. 2018a), that could originate in a post-shock region of the accretion column above the NS surface. Magnetic fields of $\sim 10^{14}$ G or larger can produce high isotropic luminosities in the accretion column (up to 2–3 orders of magnitude higher than the ordinary Thomson Eddington limit), as shown by semi-analytical calculations and 2D radiation-hydro-simulations of accretion on to NSs with large magnetic fields (Mushtukov et al. 2015, 2017; Kawashima et al. 2016).

The ULX population has continuously increased during the years reaching several hundreds known examples, although only a few of them have high-enough quality X-ray data to perform deep investigations. Here we report on two ULXs in the galaxy NGC 925 (SAB(s)d, $D \sim 8.5$ Mpc; Fig. 1). These are NGC 925 ULX-1 (CXO J022727+333443, ULX-1 hereafter) and ULX-2 (CXO J022721+333500, ULX-2 hereafter), both listed in the *Chandra* ULX catalogue (Swartz et al. 2011). ULX-1 is located in a spiral arm, while ULX-2 is at ∼80 arcsec from ULX-1. Both sources were observed 18 times by *Swift*/*XRT*, which showed that ULX-1 presented flux variations up to a factor of 3, with a peak 0.3–10 keV luminosity of $\sim 4 \times 10^{40}$ erg s^{-1} (ULX-2 was instead below the XRT threshold). Heida et al. (2016) analysed their infrared emission and estimated that the ULX-1 donor star cannot be a supergiant star of spectral type F or later, while for ULX-2 a red supergiant star may be a possible companion.

From a preliminary analysis of the only public, short, *Chandra* observation of the two sources, we found that they showed hard spectra and high short-term temporal variability. Since the combination of these properties might be an indication of an accreting IMBH, in this work we investigate further the nature of both sources using new, simultaneous, high-quality *XMM–Newton* and *NuSTAR* observations.

2 DATA REDUCTION

2.1 *XMM–Newton*

An *XMM–Newton* observation of ULX-1 and ULX-2 was taken on 2017 January 18, for a total exposure time of ∼50 ks. We extracted the data obtained with the EPIC-pn and the two EPIC-MOS cameras, both of them operated in full-frame mode. We reduced the data with the SAS v15.0.0 software, selecting single- and double-pixel events (PATTERN≤4), and single- and multiple-pixel events (PATTERN≤12), for pn and MOS, respectively. We cleaned the data removing high particle background time intervals and resulting in net exposure times of ∼32 and ∼42 ks in the pn and MOS, respectively.

For the spectral and timing analysis, we extracted the background data from circular regions of 60 arcsec radius, free of sources and close to the two ULXs. The ULX data were extracted from circular regions of 35 and 22 arcsec radii for ULX-1 and ULX-2, respectively (see Fig. 1). The smaller ULX-2 radius was chosen because the source was very close to a CCD gap. We derived a total of ∼16920/13512 and ∼1643/2420 net counts in EPIC-pn/MOS for ULX-1 and ULX-2, respectively.

2.2 *NuSTAR*

We also obtained a ∼42 ks *NuSTAR* observation which started ∼20 min before the *XMM–Newton* one, thus broadly overlapping with it. The *NuSTAR* data were reduced using the standard pipeline, based on NUSTARDAS (the *NuSTAR Data Analysis Software* v1.3.0) in theHEASOFT FTOOLS v6.16 and CALDB version 20180312. We obtained cleaned event files by applying standard procedures. We extracted the ULX-1 data, selecting a circular region of 50 arcsec radius centred on the source. The background was chosen from a nearby circular region, free of sources, of 80 arcsec radius. We obtained a total of ∼2300 net counts in the sum of the data from the FMPA and FMPB instruments. Although ULX-2 was very faint for *NuSTAR* and also close to ULX-1, a circular region of 30 arcsec was used to extract ULX-2 data in order to avoid strong ULX-1 contamination.

2.3 *Chandra*

We analysed an archival *Chandra*/ACIS-S observation (Obs.ID. = 7104) of 2005 November 23 with an exposure time of ∼2.2 ks. *Chandra* data were reduced with CIAO v.4.9 and calibration files CALDB v.4.7.6. The source events were chosen from circular regions of 3 arcsec radius (adequate for the off-axis position of the sources; see Fig. 1), while the background events were selected in a close circular region of 15 arcsec radius. We extracted the source spectra with the CIAO task SPECEXTRACT, which generates the appropriate response and auxiliary files for the spectral analysis.

The *NuSTAR* spectra were grouped with at least 100 counts per bin while the *XMM–Newton* and *Chandra* spectra were grouped with 25 counts per bin, so that minimum χ^2 fitting techniques could be used.

Model fitting was carried out using XSPEC v.12.8.2 (Arnaud 1996). The spectra of the pn and the two MOS cameras, and (when available) of the *NuSTAR* detectors were fit together. A multiplicative factor was included to account for possible inter-calibration uncertainties that, as expected, we found to be smaller than 12 per cent (e.g. Madsen et al. 2017). *Chandra* was instead analysed separately as it was not simultaneous with the other two data sets. For the spectral fits, we considered the 0.3–10 keV energy range for *Chandra* and EPIC data, and 3–70 keV energy range for *NuSTAR* data.

2.4 Optical data

On 2018 March 25, starting at 18:44:31.3 UTC, we took two images (300s + 200s) of the field of ULX-1/ULX-2 in the Hα band with the 1.8-m Copernico Telescope at Cima Ekar (Asiago, Italy). They were reduced and analysed using standard software and procedures (bias and flat field subtraction, astrometric calibration).

We report in this section that both ULX-1 and ULX-2 are surrounded by a diffuse emission in Hα, although the quality of the two images does not allow us to investigate the optical emission in deeper detail.

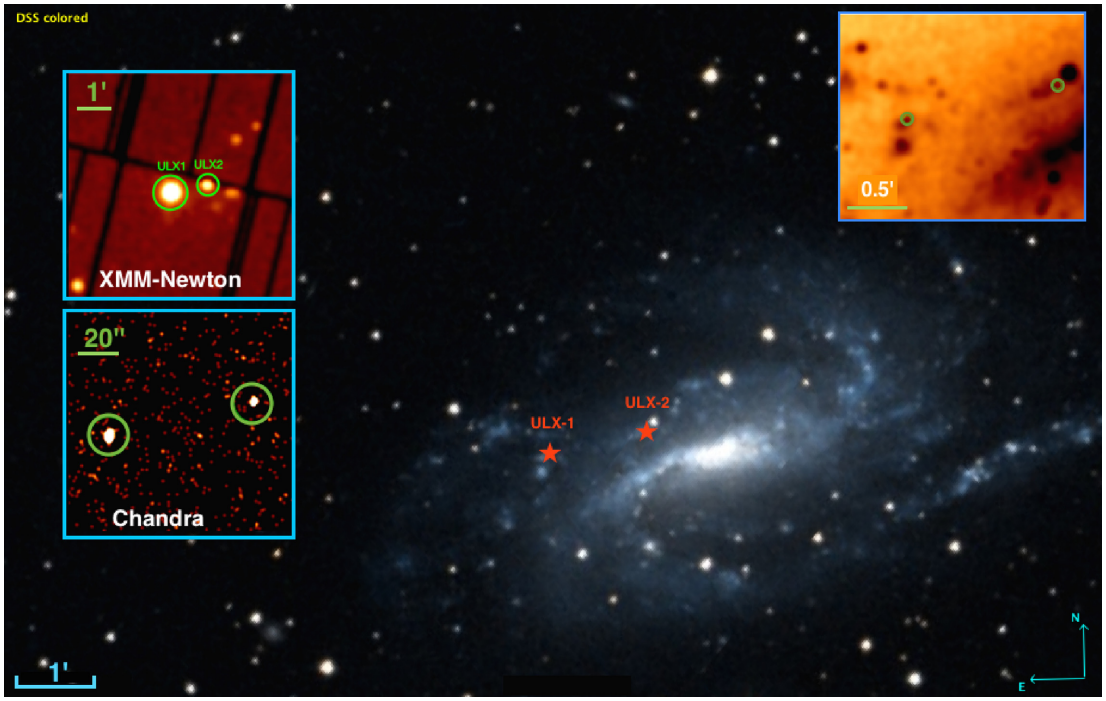

Figure 1. Digitized Sky Survey (DSS) image of the galaxy NGC 925, where the red stars indicate the positions of ULX-1 and ULX-2. Insets: *XMM–Newton*/EPIC-pn (left-top), *Chandra*/ACIS-S (left-bottom), and DSS images (right). The images have different scales.

3 DATA ANALYSIS AND RESULTS

3.1 ULX-1

3.1.1 Spectral analysis

The low counting statistics *Chandra* spectrum of ULX-1 can be modelled equally well with either an absorbed DISKBB or POWERLAW model. The POWERLAW gives a photon index $\Gamma = 1.73 \pm 0.35$, a column density of $N_{\rm H} = (0.4 \pm 0.2) \times 10^{22}$ cm^{-2}, and a 0.3–10 keV absorbed flux of $(2.10 \pm 0.35) \times 10^{-12}$ erg cm^{-2} s^{-1}.

Although this spectral shape is reminiscent of the *hard* state of XRBs (McClintock & Remillard 2006), such a possibility is ruled out when fitting the *XMM–Newton+NuSTAR* spectra. These show that the ULX-1 spectral properties are more complex than a simple DISKBB (χ^2/dof = 2013.74/980) or a POWERLAW (χ^2/dof = 1060.91/980, only marginally acceptable). We found that higher significance fits are indeed obtained with a modified accretion disc (DISKPBB), a powerlaw modified by an exponential cut-off (HIGHECUT×POWERLAW), a Comptonization model (NTHCOMP, Zdziarski, Johnson & Magdziarz 1996), or a DISKBB+BBODY (Table 1). However, the latter showed a degeneracy in the spectral parameters, allowing for both a low and high DISKBB temperature (see Table 1). The residuals of the cold-disc fit show a clear excess above 10 keV as observed in other ULXs (see e.g. Walton et al. 2018b). On the other hand, the inner disc radius estimated from the fit with a DISKPBB model is <6 km (for an inclination angle <60°) which is unphysical.

Focusing on the best fit with the NTHCOMP model (Fig. 2, top), which has the lowest χ^2_ν value, we found a column density of $(0.24 \pm 0.05) \times 10^{22}$ cm^{-2}, a photon index of 1.78 ± 0.03, and seed photons and electron temperatures of 0.15 ± 0.04 keV and 3.5 ± 0.4 keV, respectively. The seed photon temperature is quite low. Although not requested by the data, we added a DISKBB component fixing the temperature to that of the seed photons, as done in the past for a number of ULX spectra. The fit was, as expected, acceptable, with spectral parameters consistent with the single NTHCOMP model, where the seed photon temperature converged to 0.2 ± 0.05 keV. Such a low temperature is consistent with the ones inferred from other bright ULXs when fitted with the adopted model (e.g. Stobbart, Roberts & Wilms 2006; Gladstone et al. 2009; Pintore & Zampieri 2012; Pintore et al. 2014; Middleton et al. 2015), indicating that ULX-1 is not remarkably different from the rest of the bright ULX population. In addition, leaving the inner disc temperature free to vary, we also found a good fit with a seed photon and disc temperature of 0.5 ± 0.2 and 0.31 ± 0.08 keV, respectively. Because of the uncertainty in modelling the low energy part of the spectrum, the constraints on the seed photon temperature obtained with the NTHCOMP model only should be treated with caution.

The average absorbed 0.3–50 keV flux is $(2.50 \pm 0.06) \times 10^{-12}$ erg cm^{-2} s^{-1}, consistent with the average source flux during the *Chandra* observation. For a distance of 8.5 Mpc, the unabsorbed 0.3–50 keV luminosity is $\sim 2.7 \times 10^{40}$ erg s^{-1}.

3.1.2 Timing analysis

The light curve of ULX-1 indicates a 30 per cent increment in the source luminosity of the source luminosity during the *XMM–Newton* and *NuSTAR* observations. The *Chandra* light curve is instead rather constant and consistent with the flux at the beginning of the *XMM–Newton* observation (see Fig. 3). The EPIC light curve of ULX-1 shows also some high short-term variability. We split the 0.3–10 keV energy range in several intervals (0.3–0.5, 0.5–0.7, 0.7–1.0, 1.0–1.3, 1.3–2.0, 2.0–3.0, 3.0–4.0, 4.0–5.0, 5.0–6.0, 6.0–7.0, 7.0–8.0, and 8.0–10 keV) and for each of them we calculated the root mean square (rms) variability. We found that the rms fractional

Table 1. Spectral parameters for ULX-1 and ULX-2 in the *XMM–Newton+NuSTAR*. Errors are at 90percent confidence level. The fits with χ^2/dof values in boldface are statistically acceptable (null hypothesis probability higher than 2σ).

	$N_{\rm H}$ (10^{22} cm^{-2})	$kT_{\rm disk}$ (keV)	p	$N_{\rm disk}$ (10^{-5})	$kT_{\rm bb}/kT_{\rm seed}$ (keV)	$N_{\rm bb}$ (10^{-6})	Γ	$E_{\rm f}$ (keV)	$E_{\rm c}$ (keV)	$N_{pow/\rm NTHCOMP}$ (10^{-5})	χ^2/dof
ULX-1											
DISKBB	$0.079^{+0.006}_{-0.006}$	$1.69^{+0.04}_{-0.04}$	–	1266^{+110}_{-98}	–	–	–	–	–	–	2014/980
POWERLAW	$0.32^{+0.01}_{-0.01}$	–	–	–	–	–	$1.83^{+0.03}_{-0.03}$	–	–	45^{+1}_{-1}	1061/980
DISKPBB	$0.30^{+0.01}_{-0.01}$	$5.8^{+0.6}_{-0.5}$	$0.531^{+0.004}_{-0.004}$	$2.9^{+1.2}_{-1.0}$	–	–	–	–	–	–	**970/979**
BBODY+DISKBB	$0.13^{+0.02}_{-0.02}$	$2.9^{+0.2}_{-0.1}$	–	160^{+30}_{-30}	$0.34^{+0.02}_{-0.02}$	$5.8^{+0.3}_{-0.3}$	–	–	–	–	**1030/978**
BBODY+DISKBB ALT.	$0.18^{+0.01}_{-0.01}$	$0.74^{+0.04}_{-0.04}$	–	$2.0^{+0.5}_{-0.4}\times10^{4}$	$2.0^{+0.1}_{-0.1}$	$18.7^{+0.8}_{-0.8}$	–	–	–	–	1068/978
HIGHECUT×POW	$0.30^{+0.01}_{-0.01}$	–	–	–	–	–	$1.78^{+0.03}_{-0.03}$	$7.8^{+1.2}_{-1.4}$	$13.4^{+4.1}_{-3}$	43^{+1}_{-1}	**962/978**
NTHCOMP	$0.24^{+0.04}_{-0.05}$	–	–	–	$0.15^{+0.04}_{-0.04}$	–	$1.78^{+0.03}_{-0.02}$	–	$3.5^{+0.4}_{-0.3}$	39^{+3}_{-3}	**953/978**
ULX-2											
DISKBB	$0.06^{+0.02}_{-0.02}$	$1.10^{+0.07}_{-0.07}$	–	830^{+230}_{-180}	–	–	–	–	–	–	282/161
POWERLAW	$0.30^{+0.03}_{-0.03}$	–	–	–	–	–	$2.14^{+0.09}_{-0.09}$	–	–	$8.0^{+0.7}_{-0.7}$	**162/161**
DISKPBB	$0.26^{+0.02}_{-0.02}$	$3.1^{+1.0}_{-0.6}$	$0.50^{+0.01}_{*}$	$3.1^{+3.9}_{-3.1}$	–	–	–	–	–	–	**166/160**
NTHCOMP	$0.21^{+0.1}_{-0.08}$	–	–	–	$0.15^{+0.05}_{-0.15}$	–	$2.07^{+0.10}_{-0.08}$	–	100 (fixed)	7^{+1}_{-1}	**160/160**
BBODY+DISKBB	$0.23^{+0.05}_{-0.04}$	$0.41^{+0.06}_{-0.05}$	–	$3.5^{+3.0}_{-1.6}\times10^{4}$	$1.2^{+0.1}_{-0.1}$	$2.0^{+0.2}_{-0.2}$	–	–	–	–	**150/159**

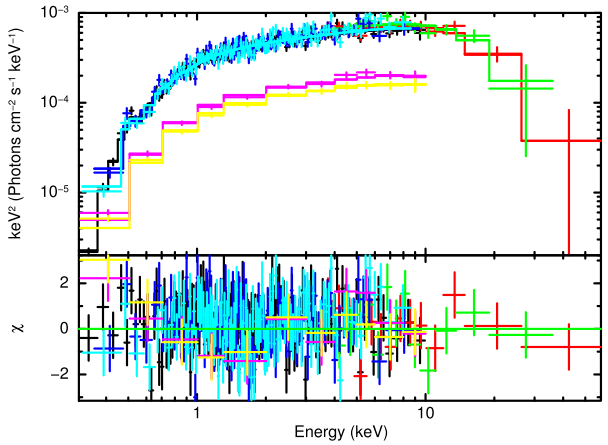

Figure 2. Unfolded $E^2f(E)$ spectra of ULX-1 fitted with an NTHCOMP model (top) and residuals (bottom), where the black, cyan, blue, red, and green points are the EPIC-pn/MOS, NUSTAR FMPA, and FMPB data, respectively. For comparison, we add the CV spectra in the top panel where the fuchsia and yellow spectra are calculated for the time-scales 300–9600 and 1000–16000 s, respectively (see Section 3.1.2).

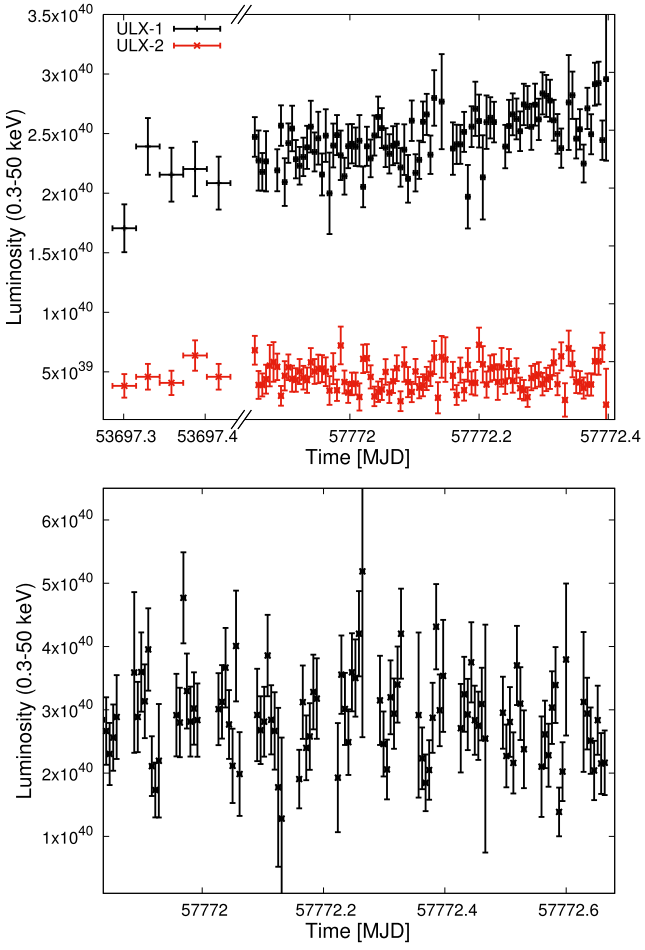

Figure 3. Top: *Chandra* (first 5 points) and EPIC-pn background-subtracted 0.3–50 keV light curve of ULX-1 (black) and ULX-2 (red), with a time binning of 500 s, obtained assuming for both *XMM–Newton* and *Chandra* data sets the best fits (Table 1) with an NTHCOMP and a BBODY+DISKBB model, respectively (see the main text). Bottom: *NuSTAR* (FMPA+FMPB) background-subtracted light curve, rebinned as the data in the top panel, and mostly overlapping in time with the EPIC-pn data.

variability (i.e. rms divided by the average count rate of each band, e.g. Vaughan et al. 2003) is ∼45 per cent in each energy band.

We further investigated such findings with the use of the covariance spectra (CV; e.g. Wilkinson & Uttley 2009; Uttley et al. 2014), which have been proven to be powerful tools to investigate the ULX timing properties (Middleton et al. 2015). We calculate the CV spectra in the same energy bands used for the rms spectrum and adopting the 1.3–2.0 keV range as reference band. We choose two overlapping time-scales to study short-term (300–9600 s) and long-term (1000–16 000 s) correlated variability. As shown in Fig. 2, both CV spectra follow the shape of the average spectrum. We fitted them with an NTHCOMP model, where we fixed all the parameters, except the normalization, to the best-fitting values of the average *XMM–Newton+NuSTAR* spectrum, and we found acceptable fits (χ^2/dof = 14.62/11 and χ^2/dof = 15.93/11, null hypothesis probability >0.14). Improvements in the best-fitting statistics can be obtained by letting also the photon index and the seed photon temperature

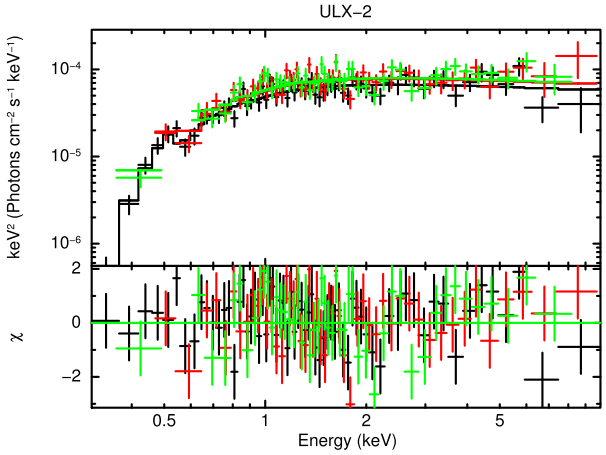

Figure 4. Unfolded $E^2f(E)$ spectra (top) and residuals (bottom) of ULX-2 when fitted with a POWERLAW model. The black, red, and green spectra are the EPIC-pn and MOS1–2 data, respectively.

free to vary, but their uncertainties make the values still consistent with those of the average spectrum. As we do not have any evidence or hint of a second spectral component in the CV spectra, these results imply that the variability is mainly driven by a single spectral component.

We also performed an accelerated search for coherent signals in the *XMM–Newton* and *NuSTAR* data, where we corrected the arrival times of the events in a grid of about 600 $\dot{P}/P$ values in the range $(\pm)$ 10^{-11}–10^{-5} s s^{-2}. The search gave no statistically significant signals, and yielded a 3σ upper limit on the fractional amplitude of 15 per cent in the period range 0.146–100s.

3.2 ULX-2

We found that ULX-2 showed a constant light curve during both *Chandra* and *XMM–Newton*/*NuSTAR* observations (Fig. 3).

We first fitted its *Chandra* spectrum with an absorbed POWERLAW, where we fixed the column density at 0.3×10^{22} cm^{-2} (see below). This model gives a photon index of 1.9 ± 0.4, again resembling a *hard* state of XRBs, and an absorbed 0.3–50 keV flux of $(7 \pm 1) \times 10^{-13}$ erg cm^{-2} s^{-1}.

However, the *XMM–Newton* data indicate that several models can provide statistically acceptable fits (see Table 1), except for a single DISKBB model (χ^2/dof = 282.3/161). The POWERLAW model is characterized by a photon index of $\Gamma = 2.14 \pm 0.09$ and a column density of 0.3×10^{22} cm^{-2} (Fig. 4). We note that the ULX-2 *NuSTAR* data are consistent with this spectral shape, although above 10 keV we found only upper limits. Instead, a fit with a DISKBB+BBODY gives a column density of 0.23×10^{22} cm^{-2} and blackbody and multicolour blackbody disc temperatures of $kT_{\rm bb} = 1.2$ keV and $kT_{\rm disc} = 0.4$ keV, respectively. The corresponding 0.3–50 keV absorbed flux is $(4.0 \pm 0.15) \times 10^{-13}$ erg cm^{-2} s^{-1}. This implies an unabsorbed 0.3–50 keV luminosity of $\sim 3.5 \times 10^{39}$ erg s^{-1} (for a distance 8.5 Mpc).

We did not find any significant short-term variability or coherent pulsation in the data. Adopting an accelerated search for coherent signals, we obtained upper limits on the fractional amplitude between 29 per centand45 per cent in the period range 0.146–100 s.

4 DISCUSSION

We have obtained the first high-quality spectral data of the two ULXs in the galaxy NGC 925, which were considered promising IMBH candidates on the basis of archival low statistics *Chandra* spectra.

4.1 ULX-2

We cannot draw firm conclusions on the nature of the compact object in ULX-2. In fact, its spectral properties are certainly not consistent with the thermal soft state of XRBs but, at the same time, they only marginally resemble those of a *hard* state (as the best-fitting power law may be too steep, $\Gamma \sim 2.1$). We found that the ULX-2 spectrum could also be modelled equally well by the combination of two thermal components (a multicolour disc plus a blackbody). Assuming an inclination angle $<60^\circ$ (suggested by the absence of dips or eclipses) and a distance of 8.5 Mpc, we estimate an inner disc radius of $\sim$500–700 km from the DISKBB normalization. A rough estimate of the BBODY emission gives instead an emitting radius of 73 ± 13 km. In the scenario of super-Eddington accretion, the former may be associated with the size of the region where outflows are ejected, while the latter might be the inner disc. Should the accreting compact object be a NS, these findings would allow us to exclude that the ULX-2 spectral components in the 0.3–10 keV energy band can be associated with the surface emission of the NS. Finally, we also note, from the optical observations, that ULX-2 is surrounded by a region of diffuse emission in Hα whose origin is not clear. Hence, further and deeper X-ray and optical observations of this source are strongly needed to better constrain its nature.

4.2 ULX-1

The high statistics obtained for ULX-1 allowed us some clearer insights on its nature. Assuming that the sub-Eddington accretion on to an IMBH shows the same states of the Galactic BH binaries, our results indicate that the IMBH scenario can be excluded while a super-Eddington accretion on to a stellar compact object appears more likely. In fact, its *XMM–Newton*+*NuSTAR* spectra revealed that the source has a very hard spectral shape but with a significant high energy cut-off. These spectral properties can be associated with a single optically thick Comptonization component, with electron temperature of $\sim$3.5 keV and seed photon temperature of 0.15 keV. Such a spectral shape allows us to classify ULX-1 as a *broadened disc* ULXs (Sutton et al. 2013b). Its measured X-ray luminosity during the *XMM–Newton* and *NuSTAR* observations was $\sim 2.5 \times 10^{40}$ erg s^{-1}. However, analysing the archival *Swift/XRT* observations[1] and assuming no significant spectral changes, we found that ULX-1 reached a peak luminosity up to $\sim 4 \times 10^{40}$ erg s^{-1}, making ULX-1 the brightest known ULXs. We note that other sources with luminosities exceeding 10^{40} erg s^{-1} present similar properties (e.g. NGC 470 ULX-1, Circinus ULX5, NGC 5907 X-1, NGC 5643 X-1; Sutton et al. 2012, 2013a; Walton et al. 2013b; Pintore et al. 2016). Following Pintore et al. (2017), we compared the position of ULX-1 with those of other well-studied ULXs on an X-ray colour–colour diagram [*softness* = (2–4 keV)/(4–6 keV), *hardness* = (6–30 keV)/(4–6 keV)]. We found that the position of ULX-1 on this hardness versus softness diagram (Fig. 5) is close to that of the PULXs. If we assume that hard ULX spectra may be

[1]We used the online tool, http://www.swift.ac.uk/user_objects/; Evans et al. (2009).

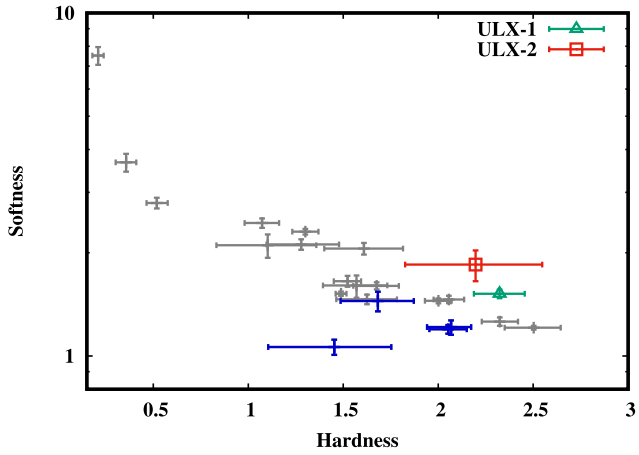

Figure 5. Colour–colour diagram obtained from the ratios of the fluxes in the energy ranges 2–4, 4–6, and 6–30 keV and calculated from the best-fitting spectral values obtained with an absorbed HIGHECUT×POWERLAW. The grey points are the sources shown in Pintore et al. (2017), while the blue points are the two PULXs NGC 5907 X-1 and NGC 7793 P13. The green triangle and the red square indicate ULX-1 and ULX-2, respectively.

associated with the PULXs, from this point of view alone we might consider ULX-1 as a possible candidate to host a NS.

Recently, Walton et al. (2018b) analysed the spectra of a sample of bright ULXs adopting a model based on super-Eddington accretion on to magnetized NSs. They showed that all spectra left an excess above 10 keV well described by a cut-off power law, the origin of which may be associated with the accretion column. This would suggest that all the ULXs of the sample can host NSs. In our analysis, we adopted a similar spectral model (DISKBB+BBODY) and we also observed an excess at high energy, which can be modelled with a cut-off power law (although not statistically required by the data). Therefore, according to this spectral model, ULX-1 can be described as another NS accreting above Eddington, where its pulsed emission would not be detected because of the strong dilution by the high disc+wind emission. According to the work of Koliopanos et al. (2017), who analysed a similar ULX sample with a similar spectral model, it would also be possible to estimate the magnetic field of the NS in ULX-1: for a high blackbody temperature of $\sim$2 keV and considering a 0.3–10 keV unabsorbed luminosity of $\sim 2 \times 10^{40}$ erg cm^{-2} s^{-1}, the magnetic field should be $\sim 5 \times 10^{13}$ G.

ULX-1 showed also high short-term variability which rules out the scenario of a stable advection dominated disc (unless it was patchy; Miller et al. 2014). The rms and covariance spectra showed that the strong variability does not depend on the energy, supporting the hypothesis that it originates in a single component. Combining the ULX-1 spectral and temporal properties, we suggest that the source is seen at small inclination angles and, if the accretion rate is highly super-Eddington, strong (clumpy) outflows are ejected. Magnetohydrodynamic simulations (e.g. Kawashima et al. 2012) indicate that such outflows create a funnel around the central compact object. We probably see the hard X-ray emission produced in the regions very close to the compact object through such a funnel (see e.g. Middleton et al. 2015). In addition, the high level of short-term variability may be produced by the clumps of the outflow that occasionally cross our line of sight towards the central regions. The existence of powerful winds around ULX-1 is supported by the properties of its infrared counterpart: Heida et al. (2016) found that the IR emission is characterized by several emission features (where the Fe II is the dominant one), likely having their origin in an extended nebula around ULX-1 which is possibly fed by the ULX outflows. This interpretation is supported by our optical observations that show clear diffuse Hα emission around the source. Deeper observations in the optical band are definitely needed to constrain the origin of such a diffuse emission.

ACKNOWLEDGEMENTS

This work is partly based on observations collected at the Copernico telescope (Asiago, Italy) of the INAF – Osservatorio Astronomico di Padova, on observations obtained with *XMM–Newton*, an ESA science mission with instruments and contributions directly funded by ESA Member States and NASA, and the NASA mission *NuSTAR*. FP and SM acknowledge the 'Contratto ASI – INAF per analisi dati NuSTAR'. PE acknowledges funding in the framework of the NWO Vidi award A.2320.0076. GR and GLI acknowledge that this research was supported in part through high performance computing resources and support provided by CINECA (MARCONI), awarded under the ISCRA initiative; and also through the INAF – CHIPP high performance computing project resources and support.

REFERENCES

Arnaud K. A., 1996, in Jacoby G. H., Barnes J., eds, ASP Conf. Ser. Vol. 101, Astronomical Data Analysis Software and Systems V (XSPEC: The First Ten Years). Astron. Soc. Pac., San Francisco, p. 17
Bachetti M. et al., 2013, ApJ, 778, 163
Bachetti M. et al., 2014, Nature, 514, 202
Caballero-Garcia M. D., Belloni T., Wolter A., 2013, MNRAS, 435, 2665
Carpano S., Haberl F., Maitra C., Vasilopoulos G., 2018, MNRAS, 476, 45
Colbert E. J. M., Mushotzky R. F., 1999, ApJ, 519, 89
Evans P. A. et al., 2009, MNRAS, 397, 1177
Fabbiano G., 1989, ARA&A, 27, 87
Feng H., Soria R., 2011, New Astron. Rev., 55, 166
Fürst F. et al., 2016, ApJ, 831, L14
Fürst F., Walton D. J., Stern D., Bachetti M., Barret D., Brightman M., Harrison F. A., Rana V., 2017, ApJ, 834, 77
Gladstone J. C., Roberts T. P., Done C., 2009, MNRAS, 397, 1836
Heida M., Jonker P. G., Torres M. A. P., Roberts T. P., Walton D. J., Moon D.-S., Stern D., Harrison F. A., 2016, MNRAS, 459, 771
Heil L. M., Vaughan S., Roberts T. P., 2009, MNRAS, 397, 1061
Israel G. L. et al., 2017a, Science, 355, 817
Israel G. L. et al., 2017b, MNRAS, 466, L48
Kaaret P., Feng H., Roberts T. P., 2017, ARA&A, 55, 303
Kawashima T., Ohsuga K., Mineshige S., Yoshida T., Heinzeller D., Matsumoto R., 2012, ApJ, 752, 18
Kawashima T., Mineshige S., Ohsuga K., Ogawa T., 2016, PASJ, 68, 83
Koliopanos F., Vasilopoulos G., Godet O., Bachetti M., Webb N. A., Barret D., 2017, A&A, 608, A47
Liu J.-F., Bregman J. N., Bai Y., Justham S., Crowther P., 2013, Nature, 503, 500
Madau P., Rees M. J., 2001, ApJ, 551, L27
Madsen K. K., Beardmore A. P., Forster K., Guainazzi M., Marshall H. L., Miller E. D., Page K. L., Stuhlinger M., 2017, AJ, 153, 2
McClintock J. E., Remillard R. A., 2006, in Levin W. H. G., van der Klis M., eds, Compact Stellar X-ray Sources. Cambridge Univ. Press, Cambridge, p. 157
Middleton M. J., Heil L., Pintore F., Walton D. J., Roberts T. P., 2015, MNRAS, 447, 3243
Miller M. C., Hamilton D. P., 2002, MNRAS, 330, 232
Miller J. M., Bachetti M., Barret D., Harrison F. A., Fabian A. C., Webb N. A., Walton D. J., Rana V., 2014, ApJ, 785, L7
Mizuno T. et al., 2007, PASJ, 59, 257
Motch C., Pakull M. W., Soria R., Grisé F., Pietrzyński G., 2014, Nature, 514, 198

Mushtukov A. A., Suleimanov V. F., Tsygankov S. S., Poutanen J., 2015, MNRAS, 454, 2539
Mushtukov A. A., Suleimanov V. F., Tsygankov S. S., Ingram A., 2017, MNRAS, 467, 1202
Ohsuga K., Mineshige S., Mori M., Kato Y., 2009, PASJ, 61, L7
Pinto C., Middleton M. J., Fabian A. C., 2016, Nature, 533, 64
Pintore F., Zampieri L., 2012, MNRAS, 420, 1107
Pintore F., Zampieri L., Wolter A., Belloni T., 2014, MNRAS, 439, 3461
Pintore F., Zampieri L., Sutton A. D., Roberts T. P., Middleton M. J., Gladstone J. C., 2016, MNRAS, 459, 455
Pintore F., Zampieri L., Stella L., Wolter A., Mereghetti S., Israel G. L., 2017, ApJ, 836, 113
Portegies Zwart S. F., Baumgardt H., Hut P., Makino J., McMillan S. L. W., 2004, Nature, 428, 724
Poutanen J., Lipunova G., Fabrika S., Butkevich A. G., Abolmasov P., 2007, MNRAS, 377, 1187
Rana V. et al., 2015, ApJ, 799, 121
Roberts T. P., 2007, Ap&SS, 311, 203
Stobbart A.-M., Roberts T. P., Wilms J., 2006, MNRAS, 368, 397
Sutton A. D., Roberts T. P., Walton D. J., Gladstone J. C., Scott A. E., 2012, MNRAS, 423, 1154
Sutton A. D., Roberts T. P., Gladstone J. C., Farrell S. A., Reilly E., Goad M. R., Gehrels N., 2013a, MNRAS, 434, 1702
Sutton A. D., Roberts T. P., Middleton M. J., 2013b, MNRAS, 435, 1758
Swartz D. A., Soria R., Tennant A. F., Yukita M., 2011, ApJ, 741, 49
Takeuchi S., Ohsuga K., Mineshige S., 2013, PASJ, 65, 88
Uttley P., Cackett E. M., Fabian A. C., Kara E., Wilkins D. R., 2014, A&AR, 22, 72
Vaughan S., Edelson R., Warwick R. S., Uttley P., 2003, MNRAS, 345, 1271
Walton D. J., Miller J. M., Harrison F. A., Fabian A. C., Roberts T. P., Middleton M. J., Reis R. C., 2013a, ApJ, 773, L9
Walton D. J. et al., 2013b, ApJ, 779, 148
Walton D. J. et al., 2014, ApJ, 793, 21
Walton D. J. et al., 2018a, MNRAS, 473, 4360
Walton D. J. et al., 2018b, ApJ, 856, 128
Wilkinson T., Uttley P., 2009, MNRAS, 397, 666
Zampieri L., Roberts T. P., 2009, MNRAS, 400, 677
Zdziarski A. A., Johnson W. N., Magdziarz P., 1996, MNRAS, 283, 193

This paper has been typeset from a TEX/LATEX file prepared by the author.